Astrocytic Nrf2 Expression Protects Spinal Cord From Oxidative Stress in a Spinal Cord Injury Animal Model

Weiyi Zhao
Universitätsklinikum Aachen: Universitatsklinikum Aachen
Natalie Gasterich
Uniklinik RWTH Aachen: Universitatsklinikum Aachen
Tim Clarner
Uniklinik RWTH Aachen: Universitatsklinikum Aachen
Clara Voelz
Universitatsklinikum Aachen
Victoria Behrens
Neuroanatomy
Cordian Beyer
Uniklinik RWTH Aachen: Universitatsklinikum Aachen
Athanassios Fragoulis
Uniklinik RWTH Aachen: Universitatsklinikum Aachen
Adib Zendedel (azendedel@ukaachen.de)
Neuroanatomy https://orcid.org/0000-0001-7415-9346

Research

Keywords: Spinal cord injury, SCI, Keap1, Nrf2, Astrocytes

Posted Date: November 9th, 2021

DOI: https://doi.org/10.21203/rs.3.rs-1030266/v1

Abstract

Background

Spinal cord injury (SCI) induces a multitude of deleterious processes, including neuroinflammation and oxidative stress (OS) which contributed to neuronal damage and demyelination. Recent studies have suggested that increased formation of reactive oxygen species (ROS) and the consequent OS are critical events associated with SCI. However, there is still little information regarding the impact of these events on SCI. Astrocytes are key regulators of oxidative homeostasis in the CNS and astrocytic antioxidant responses promote the clearance of oxidants produced by neurons. Therefore, dysregulation of astrocyte physiology might largely contribute to oxidative damage. Nuclear factor erythroid 2-related factor 2 (Nrf2) is the main transcriptional regulator of cellular anti-oxidative stress responses.

Methods

In the current study, using mice with a GFAP-specific kelch-like ECH-associated protein 1 (Keap1)-deletion, we induced a hyperactivation of Nrf2 in astrocytes and further its effects on SCI outcomes. SCI-induction was performed in mice using the Infinite Horizon Spinal Cord Impactor with a force of 60 kdyn. To assess the quantitative pattern of Nrf2/ARE-activation, we included transgenic ARE-Luc mice. Data were analyzed with GraphPad Prism 8 (GraphPad Software Inc., San Diego, CA, USA). Brown-Forsythe test was performed to test for equal variances and normal distribution was tested with Shapiro-Wilk.

Results

In ARE-Luc mice, a significant induction of luciferase-activity was observed as early as 1 day post injury, indicating a functional role of Nrf2-activity at the epicenter of SCI. Further, SCI induced loss of neurons and oligodendrocytes, demyelination and inflammation in wild type mice. The loss of myelin and oligodendrocytes was clearly reduced in Keap1 KO mice. In addition, Keap-1 KO mice showed a significantly better locomotor function and lower neuroinflammation responses compared to wild type mice.

Conclusions

In summary, our *in vivo* bioluminescence data showed Nrf2-ARE activation during primary phase of SCI. Further, we found that cell specific hyperactivation of Nrf2 was sufficient to protect the spinal cord against injury which indicate a promising therapeutic approach for SCI-treatment.

Background

Spinal cord injury (SCI) characteristically causes life-long neurological consequences such as paralysis, loss of sensation and voluntary motor function downwards the site of injury which remains a major cause of permanent disability (1). SCI is divided into primary and secondary injuries in a pathophysiological classification; primary injury refers to the initial physical damage of the spinal cord

(SC) caused by an indirect or direct external force, while the secondary injury is described by a series of physiological and pathological changes including neuroinflammation, neuronal apoptosis and excessive occurrence of oxidants such as reactive oxygen species (ROS) (2). However, oxidants are not necessarily harmful *per se* but do also play important roles at low exposition rates during redox-related signaling cascades by which they regulate and participate in physiological processes (thoroughly reviewed by Sies and Jones in 2020 (3)). The redox homeostasis under these circumstances should be understood as a range rather than a clearly defined intracellular state in which the ratio of oxidants and antioxidants within the cell is in dynamic equilibrium with a pending electron flow, a condition that is called oxidative eustress (4-6). Nevertheless, once endogenous antioxidants are overwhelmed by an increased occurrence of oxidants, exceeding the limits of homeostatic conditions, a harmful imbalance between products of oxidation and antioxidant defenses results, known as oxidative distress (OS) (7). Besides, oxidative damage to proteins and DNA, these oxidants attack polyunsaturated fatty acids in the membrane lipids, change membrane potentials and eventually rupture membranes leading to the release of cell and organelle contents (8). Neurons are particularly prone to oxidative and electrophilic distress due to many factors, including a high content of polyunsaturated fatty acids, high rate of oxidative metabolic activity, intense production of reactive oxygen metabolites and relatively low antioxidant capacity (9). Although increased OS is an important hallmark of the secondary phase of SCI (10), there is still little information about the impact of this biochemical changes associated with SCI outcome.

Astrocytes are the most abundant glial cells in the central nervous system (CNS) and among the first responders to SCI (11). After SCI, local environment undergoes profound biochemical and cellular changes that affect astrocytes to become reactive and include astrogliosis (12). Reactive astrogliosis is characterized by the proliferation and hypertrophy of astrocytes, which eventually leads to scar formation in epicenter of injury post SCI (13). Astrocytes play critical roles in the normal SC; they closely interact with neurons to provide structural, metabolic and trophic support and actively participate in the modulation of neuronal excitability and neurotransmission (14). In the presence of astrocytes, neurons are more resistant to OS induced by several compounds (15). Astrocytes carry out this function mainly through transcription factor nuclear factor erythroid 2-related factor 2 (Nrf2)-driven genes such as quinone oxidoreductase 1 (NQO1) and heme oxygenase-1 (HO-1) which are both preferentially activated in astrocytes but lesser in neurons (16). Therefore, functional alterations in astrocytes (such as aggravation of OS) can shape and alter their interaction with neurons.

Nrf2, belonging to the cap ‘n’ collar subfamily of basic region-leucine zipper transcription factors, is the main transcription factor involved in the regulatory cascades during oxidative eustress responsible for the regulation of a whole battery of cytoprotective and antioxidative proteins by binding to antioxidant response elements (ARE) in their promoter region (17, 18). The activity of Nrf2 is negatively regulated by the cytosolic regulatory protein kelch-like ECH-associated protein 1 (Keap1) (19). Once, cells are exposed to OS or chemopreventive factors, Nrf2 is dissociated from Keap1, translocated into the nucleus, and induces the expression and up-regulation of downstream cytoprotective enzymes that attenuate tissue injury (20). Since, Nrf2 is rapidly degraded through interactions with Keap1, increased Nrf2 expression does not necessary lead to increased Nrf2 activity (21). Nrf2-inducers such as pharmacological activation

of the Nrf2/ARE system is a pathway which leads to increased Nrf2-signaling. For example, treatment with dimethyl fumarate (DMF) results in beneficial effects in different CNS diseases, such as multiple sclerosis (22) and SCI (23). Although the mechanism of action is not completely understood, it has been shown that dimethyl fumarate (DMF) induces Nrf2-activity by disruption of the Nrf2-Keap1 interaction due to a modification of the Keap1 protein (24). However, all known Nrf2-inducers not only enhance Nrf2-activity but also exert various side effects within the brain and other peripheral tissues (25). Therefore, genetic and cell type-specific targeting of Keap1 and Nrf2 represents the most suitable method to investigate Nrf2-specific effects. In the current study using *GFAP-Cre::keap1*$^{flox/flox}$ KO mouse, we induced hyper-activation of the Nrf2/ARE system in astrocytes in a SCI model and investigated the protective effects of astrocyte-specific Nrf2/ARE-activation in the SC after SCI.

Methods

Animals

All experimental procedures and animal care were approved by the review board for the care of animal subjects of the district government (LANUV, Germany) and are reported in accordance with the ARRIVE guidelines. The mice were housed and handled in accordance with the guidelines of the Federation for European Laboratory Animal Science Associations (FELASA) under standard laboratory conditions.

The following mouse strains were included in this study: 1. C57BL/6J ARE luciferase reporter gene mice (Cgene, Oslo) (26) to visualize Nrf2-activation in epicenter of SC (7 days); 2. *GFAP-Cre::keap1*$^{flox/flox}$ KO (in this manuscript is referred to as Keap1-KO) mice were generated by cross-breeding of GFAP-Cre expressing mice with Keap1$^{loxP/loxP}$ mice as described in detail before (27) and 3. C57BL/6J wild-type mice.

Spinal cord injury

General anesthesia was initiated with isoflurane (2-3 vol. %) in an anesthetic chamber. During surgery, isoflurane (1,5-2 vol. %) was further administered via a face mask. Intraoperative analgesia was attained through injection of buprenorphine (0.05-1 mg/kg sc.) 30 min preoperatively. After the exposure of the spinal column (Th7-Th10), a laminectomy of Th8 was performed (Fig. S1A). A standardized injury of the SC at this level was induced by contusion (Infinite Horizons Spinal Cord Impactor) with a force of 60 kdyn (28). During the surgery, body temperature was maintained at 36–37°C. Postoperative aftercare included rehydration (0,5 mL NaCl), postoperative analgesia and manual emptying of bladder twice a day until spontaneous urination returned. In the control group (sham), laminectomy without contusion of the SC was carried out to preclude possible falsifications of the results caused by the mere surgical procedure.

ARE activity

ARE-activity measurement were performed as previously described (27). Briefly, after shaving the back of mice, luciferin solution was prepared and used at a final concentration of 20 mg/mL. Totally, 0.2 mL

luciferin solution was injected intraperitoneal. After injection, mice were anesthetized by inhaling 4% (v/v) isoflurane at a flow rate of 2 L/min oxygen for approximately 1 min and then kept at 1.5% (v/v) and 1 L/min using a mouse face mask. To ensure an adequate distribution of Luciferin in the whole body, the measurements were conducted fifteen minutes after the injection. For each measurement, one sham and one SCI mouse was imaged simultaneously for 5 min at high-resolution settings (binning: 2, f/stop: 1) with a field of view of 7.5 cm. Luminescence signals were detected with an IVIS Lumina 100 Series Imaging device (Xenogen Corporation,vAlameda, CA), digitized and evaluated using the Living Image software 3.2. The signal intensities are expressed as average radiance (p/sec/cm²/sr) and visualized with the help of a false color scale. Spinal cord-specific Nrf2/ARE activity was determined by correcting luminescence signals from pre-defined region of interest (ROIs) using background ROI (Fig. S1B).

Functional activity

The locomotion deficits of mice after SCI were scored in an open field according to Basso, Beattie, and Bresnahan (BBB) locomotion where hindlimb function could be assessed (Basso et al., 1995). This is a 22-point scale that systematically details hindlimb function of joint movements, stepping ability, the degree of fine control of coordinated stepping and trunk stability. Test sessions were 4 min in duration and mice were tested every day, from days 1 to 7 post-injury and were scored by two experienced raters which were blinded to experimental groups.

Tissue preparation

To obtain samples for molecular biology and biochemical examinations, mice were deeply anesthetized and transcardially perfused with ice cold phosphate-buffered saline (PBS), the whole SC was quickly removed, and the epicenter part was dissected, snap-frozen in liquid nitrogen, and stored at -80°C until further experiments. For immunohistochemistry, mice were transcardially perfused with ice cold PBS followed by a 3.7% paraformaldehyde solution (PFA, pH 7.4). For decalcification, spinal columns were incubated in 20% ethylenediaminetetraacetic acid (EDTA) for 48 h at 37°C prior to paraffin embedding. To this end, tissue specimens were embedded in paraffin (Merck, Germany) and 5 µm paraffin sections were cut.

Gene expression studies

For RNA isolation, tissues were placed in homogenization tubes containing 1.4 mm ceramic beads. RNA was isolated by phenol-chloroform extraction using peqGold RNA TriFast (PeqLab, Germany). Therefore, samples were homogenized at 5.000 x g for 15 s. Total RNA amount and purity were determined with a Nanodrop 1000 photospectrometer (PeqLab, Germany) using A260/A280 as well as A260/230 ratios. cDNA was synthesized by reverse transcription using M-MLV reverse transcription (RT)-kit (Invitrogen, USA) and random hexanucleotide priming (Invitrogen, Germany). Gene expression levels were determined by real-time reverse transcription-PCR using SensiMix™ SYBR® & Fluorescein Kit (Bioline, Germany) in a CFX connect Real-Time PCR system device (Bio-Rad, Germany). Primer sequences, individual annealing temperatures (AT), expected amplicon length are shown in Table 1. Results were evaluated using Bio-Rad

CFX manager (Bio-Rad, Germany) and were normalized to a reference gene index (RGI), which was calculated from cyclophilin A and HSP90 expression data. Amplification efficiencies were calculated by standard curve analyses using a 2-fold dilution series of pooled samples. The target gene expression was calculated using efficiency corrected ΔΔCq method, using the geometric mean of both reference genes.

Table 1: List of used primers for PCR analysis, s: sense; as: anti-sense; AT: annealing temperature

primer	sequence [5′ → 3′]	AT [°C]	Amplicon length [bp]
HO-1	S: AAGCCGAGAATGCTGAGTTCA	62	100
	AS: GCCGTGTAGATATGGTACAAGGA		
GCLC	S: GGGGTGACGAGGTGGAGTA	65	125
	AS: GTTGGGGTTTGTCCTCTCCC		
Nqo1	S: CTACCCCCAGTGGTGATAGAAA	60	103
	AS: AGAGAGTGCTCGTAGCAGGAT		
Txnrd1	S: GGGCTTCCACGTGCTGGGTC	60	163
	AS: TCCCCCAGAGCGCTTCGTCA		
IL-6	S: GATACCACTCCCAACAGACCTG	65	122
	AS: GGTACTCCAGAAGACCAGAGGA		
TNF-a	S: GCCATAGAACTGATGAGAGGGAG	62	139
	AS: GGTGCCTATGTCTCAGCCTCTT		
CXCL10	S: CCAAGTGCTGCCGTCATTTTC	64	86
	AS: GGCTCGCAGGGATGATTTCAA		
IL-1b	S: GCCCATCCTCTGTGACTCAT	61	230
	AS: AGGCCACAGGTATTTTGTCG		
Cyclophilin A	S: TTGGGTCCAGGAATGGCAAGA	64	148
	AS: ACATTGCGAGCAGATGGGGT		
Hsp90	S: TACTACTACTCGGCTTTCCCGT	64	191
	AS: TCGAATCTTGTCCAGGGCATC		

Protein biochemical analysis

Isolated tissues were mechanically disrupted in radioimmunoprecipitation assay (RIPA) buffer (pH 8.0) supplemented with a protease inhibitor cocktail (Complete Mini, Roche Diagnostics, Grenzach-Wyhlen, Germany). Protein concentrations were determined using the PierceTM BCA protein assay kit (Thermo

Fisher Scientific, Waltham, USA) according to the manufacturer's protocol. Same amounts of protein samples (approx. 20 µg per lane) were loaded, separated in a 12% SDS polyacrylamide gel by gel electrophoresis and transferred to a PVDF (polyvinylidene difluoride) membrane. After blocking with 5 % skimmed milk in Tris-buffered saline containing 0.05 % Tween 20 (TBS-T) for 1 h at room temperature, polyvinylidene difluoride (PVDF) membranes were incubated with primary antibodies (Table 2) overnight at 4°C. An appropriate secondary antibody (1:5.000, see Table 2) was applied for 2 h at room temperature. Signals were analyzed via chemiluminescence detection (Westar Supernova, XLS 3,0100, Cyanagen, Italia), visualized (Fusion Solo X, Vilber, Germany) and subjected to densitometry analysis using Image J. Results were normalized to the expression of GAPDH or b-actin as reference protein.

Immunohistochemistry and luxol fast blue staining

For immunohistochemistry, 5 µm thick sections of SC were deparaffinized, rehydrated, and antigens were unmasked by heating in Tris/ EDTA (pH 9.0) buffer for 20 min. After blocking with 5% normal goat serum in PBS, the sections were incubated overnight at 4°C with the primary antibody diluted in blocking solution. Primary antibodies and dilutions used in the study are given in Table 2. After washing and blocking of endogenous peroxidase with 0.3% hydrogen peroxide, slides were incubated with the appropriate secondary antibody (1:50; see Table 2) diluted in 5% normal serum in PBS for 1 h (RT). Afterwards, an incubation with ABC-solution (both parts 1:50, VECTASTAIN Elite ABC Kit (Standard), Vector Labs, PK-6100) diluted in PBS for 1 h (RT) followed. For visualization by 3'3-diaminobenzidine (DAB), the working solution (1:50, pH 7.5, DAKO, Hamburg, Germany) was applied for 10 min. Where appropriate, slides were counterstained with Mayer's Haematoxylin (1 min) to visualize cell nuclei. The sections were washed again, dehydrated and mounted.

For Luxol Fast Blue (LFB) staining, sections were deparaffinized and hydrated, then incubated in a 0.1% LFB solution overnight at 56°C. The next day, the excess of staining solution was rinsed off in 95% ethyl alcohol, washed in distilled water and differentiated in 0.05% lithium carbonate solution for 20 s. After this, periodic acid–Schiff (PAS) staining was performed by oxidizing the slides in 0.5% periodic acid solution for 5 min, rinsing in distilled water, and incubating in Schiff reagent for 15 min. Afterwards, sections were washed in tap water for 5 min. Slides were counterstained with Mayer's hematoxylin for 1 min. The tissue was then washed again, dehydrated and mounted.

Table 2: List of used antibodies

			dilution factor		
antibody	**host species**	**company**	**IHC**	**WB**	**secondary antibody, company**
HO-1	Mouse	Abcam	-----	1:200	Goat Anti-Mouse IgG, Sigma
4-HNE	Mouse	Abcam	1:2000	-----	Horse Anti-Mouse IgG, Vector
NQO1	Mouse	Thermo Fisher	-----	1:500	Goat Anti-Mouse IgG, Sigma
MBP	Rat	Abcam	-----	1:1000	Rabbit Anti-Rat IgG, abcam
Olig-2	Mouse	Millipore	1:2000	-----	Horse Anti-Mouse IgG, Vector
NeuN	Mouse	Millipore	1:5000	-----	Horse Anti-Mouse IgG, Vector
b-actin	Goat	Santa Cruz	-----	1:5000	Rabbit Anti-Goat IgG, Sigma
GAPDH	Rabbit	Santa Cruz	-----	1:5000	Goat Anti-Rabbit IgG, BIO-RAD
GFAP	Goat	Santa Cruz	1:1000	-----	Horse Anti-Goat IgG, Voctor
S100b	Rabbit	Abcam	1:10000	-----	Goat Anti-Rabbit IgG, Vector

Statistical analysis

GraphPad Prism 8 (GraphPad Software Inc., San Diego, CA, USA) was used for statistical analyses. Brown-Forsythe test was performed to test for equal variances and normal distribution was tested with Shapiro-Wilk test. If necessary, data were transformed via Box-Cox-Y to achieve homoscedasticity. One-way ANOVA followed by Dunnett post-hoc test or two-way ANOVA followed by Tukey post-hoc test was used for parametric data. Non-parametric data were analyzed with Kruskal-Wallis test followed by Dunn's multiple comparisons or Friedman test. All data are given as arithmetic means ± standard errors of the mean (SEM). p-values < 0.05 were considered significant. Detailed description of significance levels are given in the figure legends.

Results

Activation of the Nrf2/ARE pathway after SCI

To investigate whether the Nrf2/ARE system plays a role in our experimental SCI animal model and to assess the quantitative pattern of its activation, we included transgenic ARE-Luciferase reporter gene mice. In this approach, due to the ARE-driven expression of the luciferase, the luminescence intensity directly correlates with Nrf2-activity. Using the XENOGEN Living Image system, the luminescence signals in SCI and sham mice were daily measured *in vivo*. As shown in figure 1, compared to sham control animals a significant increase of luciferase activity was observed in the epicenter of SC in SCI mice as early as 24 h post injury. The luminescence intensity gradually declined during the study but remained significantly higher for up to 4 days compared to sham controls (figures 1A and B). Afterwards, the mean signal intensities of SCI mice were still higher than those of sham control animals but without reaching

statistical significance. These experiments indicate an involvement of Nrf2-activity in our contusion model of SCI. Further, to confirm *in vivo* bioluminescence analysis, we measured the expression of four typical Nrf2-target genes including heme oxygenase-1 (HO-1), glutamate-cysteine ligase catalytic subunit (GCLC), NAD(P)H dehydrogenase [quinone] 1(NQO1) and thioredoxin reductase-1(TXNRD1) by RT-qPCR. These results showed an induction of the gene expression of all selected genes in epicenter after SCI (figures 2 A-D). To further investigate OS, we analyzed protein levels of HO-1 and NQO1 in SC using WB. As shown in figures 2 E-G, protein expression of HO-1 and NQO1 was significantly induced as early as 12h post-OP and remained at comparable levels until day 7. These results indicate the critical role of the Nrf2-regulated anti-oxidant machinery in the early phase after SCI.

Nrf2 hyperactivation improves the functional recovery

In the next step, to investigate the effect of astrocytic Nrf2-activation on locomotor recovery after SCI, we performed the BBB scoring for 7 consecutive days after injury. During the first 5 d after insult, there was no significant difference between WT and Keap1-KO mice (figure 3 A) even if the mean score of Keap1-KO was slightly higher than the score of WT mice. At day 6 and 7 post injury, the Keap1-KO group showed a significantly higher BBB scoring compared to WT animals which indicates that increased Nrf2 activity improves the recovery of locomotor abilities in SCI mice. In a further attempt, we explored whether Nrf2-target genes are regulated in Keap1-KO mice. The RT-qPCR data revealed that mRNA expression levels of NQO1 in Keap1-KO mice were significantly higher than in WT mice at 24 and 72 h post SCI (figure 3 C), whereas, the expression level of HO-1 showed no significant changes in both mice strains (data are not shown).

Sustained elevated Nrf2/ARE pathway protects spinal cord tissue

We have shown that the activation of the Nrf2/ARE pathway in the epicenter of the SC is a characteristic feature of our SCI model. We, therefore, aimed at investigating whether a continuous hyperactivation of Nrf2 might prevent cellular pathological responses in traumatic SCI. Since astrocytes are critically involved in the maintaining of hemostasis during SCI, Keap1 was deleted specifically in this cell type, representing a genetic model for sustained activation of the Nrf2/ARE pathway in astrocytes (29).

To demonstrate its effect on the prevention of demyelination, sagittal sections of SC were stained with LFB. In sham operated mice, LFB staining of myelin in the SC was mainly restricted to the white matter (yellow arrows figure 4 E). The microscopic observations revealed that at 7 d post SCI, LFB staining was strongly reduced with almost no staining visible in the dorsal column at the center and caudal of the injury (stars in figures 4 B and F). In addition, most of the ventral column also showed a partially reduction of staining in the epicenter. In sharp contrast, the loss of myelin was significantly prevented in Keap1-KO mice in both the central and caudal parts of SC (figures 4 C and G). Since myelin basic protein (MBP) is one of the main protein known to be required for myelin assembly, we measured the amount of this protein in WT and Keap1-KO mice. Our results show that SCI significant reduced MBP in WT mice and that this effect is ameliorated in Keap1-KO animals, which also showed a decreased amount of MBP but significantly more than WT mice (figures 4 I and J).

To further examine whether the suppression of demyelination is correlated with improved survival of oligodendrocytes in Keap1-KO mice, we conducted immunohistochemical detection with anti-Olig2 (oligodendrocytes) and anti-APC (mature oligodendrocytes) antibodies. The quantifications of Olig2 immunoreactive oligodendrocytes showed that SCI induced a significant loss of Olig2- and APC-positive cells in the gray matter (figures 5 B and F). While we found higher numbers of Olig2-positive cells in Keap1-KO animals compared to WT mice after SCI (figures 5 B, C and D).To investigate whether increased astrocytic Nrf2-activity protected neurons against SCI-mediated damage, neuronal density was evaluated using immunohistochemistry against NeuN (a specific neuronal protein). We measured a significant decline of NeuN-positive cells in WT mice after SCI and a similar reduction in Keap1-Ko mice (figures 5 E-H).

Increased astrocytic Nrf2 activity ameliorates neuroinflammation after SCI

In order to determine the influence of astrocytic Nrf2 activation on neuroinflammation, mRNA expression of pro-inflammatory cytokines (IL-6, CXCL10, IL-1b and TNF-α) were analyzed in WT and Keap1-KO mice at various time points (12 h, 24 h, 72 h and 7 d) after SCI. The analyses revealed that IL-6, CXCL10 and IL-1b mRNA expressions immediately rose within the first 12 h post injury and then gradually declined up to 7 d post SCI (figures 6 A-C). However, these inflammatory factors were significantly lower at the early phase of injury (12 h) in the Keap1- KO mice in comparison to WT animals (figures 6 A-C). Moreover, TNF-α was up-regulated in the early phase of SCI and remained constantly at this high level until 7 d after SCI. The expression of this cytokine was significantly lower in knock-out mice (figure 6 D). Further, Iba-1 staining revealed a strong microgliosis in both SCI animals. However, this pathological feature was significantly attenuated in Keap1-KO mice (figures 6 E-H).

Astrocyte reactivity in Keap1-KO mice

A main characteristic feature of SCI is the accumulation of reactive astrocytes identified as astrogliosis. Therefore, our next approach was to investigate the activation of astrocytes in WT as well as Keap1-KO mice after SCI. As expected, SCI in WT mice increased the number of GFAP- (figures 7 B and D) and S100b- (figures 7 F and H) positive cells in the SC compared to sham treated animals (figures 7 A and E). This induction in epicenter was comparable in both mouse strains and was not abolished in Keap1-KO mice (figures 7 C and G). Additionally, mRNA and protein levels of GFAP were examined using RT-qPCR and WB, respectively. Although the number of GFAP-positive cells did not differ between genotypes, we observed a significant reduction of GFAP after 7 days at both the mRNA (figure 7 I) as well as the protein (figures 7 J and K) level in Keap1-KO mice compared to WT animals. This indicates that Nrf2 may rather affect the activation/reactivity of astrocytes than their proliferation.

Discussion

Spinal cord injury (SCI) has been shown to be associated with different kind of tissue damage (30). Besides others, oxidative stress has frequently been described to be involved during SCI pathogenesis (31). While oxidative eustress (low oxidant exposure) regulates a couple of intracellular redox-regulated

processes to maintain redox-homeostasis (6), oxidative distress represents an excess of oxidants leading to tissue damage. The nuclear factor erythroid-2 related factor 2 (Nrf2) regulates a battery of genes that encode for anti-oxidative enzymes that are part of eustress-related signaling. We demonstrated that the Nrf2/ARE system was activated immediately in the course of SCI-induced redox signaling. However, significant tissue damage occurs in this model despite Nrf2 activation, suggesting that the physiological Nrf2 response is insufficient to adequately counteract the full extent of this damage (32).

Fu and colleagues just recently demonstrated that luteolin pre-treatment, a flavonoid known to activate Nrf2 and to exert antioxidant properties, improved SCI-related burden in rats (33). Besides from luteolin there have been other Nrf2 activating substances been used in similar studies (34-36). However, all these studies share a common drawback that these compounds have a variety of other intracellular effects in addition to Nrf2 activation, which are not always completely known.

Astrocytes are prominent in the cellular response to SCI which maintain the neuronal structure and nutrition. Furthermore, it has been shown that astrocytes provide protection against different kind of damage, including oxidative stress (37). For this reason, a more detailed study of the role of Nrf2 specifically in astrocytes during SCI, which has not been addressed in previous studies, would be of scientific value.

Therefore, in addition to wildtype mice we used transgenic GFAP-mediated Keap1-KO mice to continuously activate Nrf2 in astrocytes. In contrast to before-mentioned studies, in which the treatment regiments induce a systemic Nrf2 activation, we were able to show that Nrf2 hyperactivation exclusively in astrocytes was absolutely sufficient to overcome SCI-related outcomes. In particular, our study revealed that besides protecting against general tissue damage (including demyelination and oligodendrocyte loss), sustained Nrf2 activity also prevented the intracellular redox milieu to switch to oxidative distress.

Neuroinflammatory response is one of the main events which occurs within early hours from the onset of SCI, which contributes to neuronal death and further neurologic damages. The neuroinflammation is mainly characterized by the infiltration of inflammatory cells such as macrophages as well as the accumulation of inflammatory mediators like IL-1b and IL-6. In this study we observed that Keap-1 KO mice showed a significantly lower expression of pro-inflammatory cytokines and also SCI-induced microgliosis, suggesting that increased astrocytic activity of Nrf2 plays a critical role in counteracting the inflammation. Even though microgliosis was clearly reduced in Keap1-KO mice, astrocyte numbers did not alter. However, in the context of neuroinflammation not simply the amount of astrocytes but rather their reactivity is crucial for tissue damage (38). Because the expression of GFAP, one of the prime markers of astrocyte reactivity, was significantly reduced in Keap1-KO mice, it is reasonable to conclude that Keap1 depletion significantly reduces the astrocyte-triggered inflammatory response, despite unchanged astrocyte numbers. This is consistent with the results of one of our previous studies showing that astrocytic Keap1-KO reduced neuroinflammation and tissue damage in a mouse model of multiple sclerosis, although the number of astrocytes also did not differ from treated WT mice (27). Several evidences confirm that Nrf2 can limit the inflammatory response by inhibiting NF-kB activation through

maintenance of redox homeostasis (39, 40). This important protective function of Nrf2 is mainly mediated through its antioxidant and detoxifying enzymes, such as NQO1. Thus, enhancement of these antioxidant systems, as is the case in astrocytes of Keap1-KO mice, could lead to decreased production of pro-inflammatory cytokines. Therefore, enhancement of these antioxidant systems, as is the case in astrocytes of Keap1-KO mice, could lead to decreased production of pro-inflammatory cytokines. This is particularly also important because, among other functions, astrocytes are responsible for maintaining a suitable environment for neurons including redox homeostasis. To ensure this, they contribute significantly to the reduction of oxidative distress by counteracting excessive accumulation of ROS in their surrounding area (41). Since increased emergence of ROS not only leads to oxidative damage of biomolecules but also activates microglial cells, astrocytes with increased antioxidant defenses may exert a direct inhibitory influence on microgliosis (41).

Conclusion

In summary, our *in vivo* bioluminescence data showed Nrf2-ARE activation during primary phase of SCI. Further, we were able to demonstrate that hyperactivation of Nrf2 improves functional recovery, prevents the neuroinflammation and demyelinating. Better understanding of underlying mechanisms of oxidative stress could help us to promote new therapeutic intervention in SCI patients.

Abbreviations

4-HNE	4-Hydroxynonenal, or trans-4-hydroxy-2-nonenal
ARE	antioxidant response element
b-actin	beta-actin
BBB	Basso, Beattie, and Bresnahan score
CNS	central nervous system
CXCL10	C-X-C motif chemokine 10
DAB	3'3-diaminobenzidine
DMF	dimethyl fumarate
EDTA	ethylenediaminetetraacetic acid
GAPDH	glyceraldehyde 3-phosphate dehydrogenase
GFAP	glial fibrillary acidic protein
Ho-1	heme oxygenase-1
Hsp90	heat shock protein 90
Iba-1	microglial marker, also called allograft inflammatory factor 1
IL-1b	interleukin-1 beta
IL-6	interleukin-6
Keap1	kelch-like ECH-associated protein 1
KO	knockout
LFB	Luxol Fast Blue
MBP	myelin basic protein
NeuN	neuronal marker, also called Hexaribonucleotide Binding Protein-3
NF-kB	nuclear factor 'kappa-light-chain-enhancer' of activated B-cells
Nqo1	NAD(P)H dehydrogenase [quinone] 1
Nrf2	nuclear factor erythroid 2-related factor 2
Olig-2	oligodendrocyte transcription factor 2
OS	oxidative stress
PAS	periodic acid–Schiff
PBS	phosphate-buffered saline
PFA	paraformaldehyde

RGI	reference gene index
RIPA	radioimmunoprecipitation assay
ROI	region of interest
ROS	reactive oxidant species
RT	room temperature
S100b	S100 calcium-binding protein B
SC	spinal cord
SCI	spinal cord injury
TBS-T	Tris-buffered saline containing 0.05 % Tween 20
TNF-a	tumor necrosis factor alpha
Txnrd1	thioredoxin reductase-1
WB	western blot

Declarations

Ethics approval and consent to participate

All experimental procedures and animal care were approved by the review board for the care of animal subjects of the district government (LANUV, Germany) and are reported in accordance with the ARRIVE guidelines.

Consent for publication

Not applicable

Availability of data and materials

The datasets analysed during the current study are available from the corresponding author on reasonable request.

Competing interests

The authors declare that they have no competing interests.

Funding

This project was supported by an internal grant from RWTH Aachen University (A. Zendedel, START-101/18) and also China Scholarship Council Foundation (Award No.20190808157).

Authors' contributions

CB, AF and AZ designed and supervised the study. WZ conducted the SCI surgical procedures, and contributed to data collection and to the preparation of the manuscript. WZ and AF conducted the longitudinal ARE *in vivo* measurements. NG, TC, CV and VB performed the histological staining and evaluation as well as gene and protein expression analyses. CB, AF and AZ analyzed and interpreted the data and were major contributor in writing the manuscript. All authors read and approved the final manuscript.

Acknowledgements

We thank Uta Zahn, Petra Ibold, and Helga Helten for their technical support.

References

1. Thuret S, Moon LD, Gage FH. Therapeutic interventions after spinal cord injury. Nat Rev Neurosci. 2006;7(8):628-43.

2. Bains M, Hall ED. Antioxidant therapies in traumatic brain and spinal cord injury. Biochim Biophys Acta. 2012;1822(5):675-84.

3. Sies H, Jones DP. Reactive oxygen species (ROS) as pleiotropic physiological signalling agents. Nat Rev Mol Cell Biol. 2020;21(7):363-83.

4. Di Meo S, Reed TT, Venditti P, Victor VM. Role of ROS and RNS Sources in Physiological and Pathological Conditions. Oxid Med Cell Longev. 2016;2016:1245049.

5. Foyer CH, Noctor G. Redox homeostasis and antioxidant signaling: a metabolic interface between stress perception and physiological responses. Plant Cell. 2005;17(7):1866-75.

6. Sies H. Hydrogen peroxide as a central redox signaling molecule in physiological oxidative stress: Oxidative eustress. Redox Biol. 2017;11:613-9.

7. Birben E, Sahiner UM, Sackesen C, Erzurum S, Kalayci O. Oxidative stress and antioxidant defense. World Allergy Organ J. 2012;5(1):9-19.

8. Su LJ, Zhang JH, Gomez H, Murugan R, Hong X, Xu D, et al. Reactive Oxygen Species-Induced Lipid Peroxidation in Apoptosis, Autophagy, and Ferroptosis. Oxid Med Cell Longev. 2019;2019:5080843.

9. Shichiri M. The role of lipid peroxidation in neurological disorders. J Clin Biochem Nutr. 2014;54(3):151-60.

10. Jia Z, Zhu H, Li J, Wang X, Misra H, Li Y. Oxidative stress in spinal cord injury and antioxidant-based intervention. Spinal Cord. 2012;50(4):264-74.

11. Seifert G, Schilling K, Steinhäuser C. Astrocyte dysfunction in neurological disorders: a molecular perspective. Nature reviews Neuroscience. 2006;7(3):194-206.

12. Fitch MT, Silver J. CNS injury, glial scars, and inflammation: Inhibitory extracellular matrices and regeneration failure. Experimental neurology. 2008;209(2):294-301.

13. Silver J, Miller JH. Regeneration beyond the glial scar. Nature reviews Neuroscience. 2004;5(2):146-56.

14. Bélanger M, Magistretti PJ. The role of astroglia in neuroprotection. Dialogues Clin Neurosci. 2009;11(3):281-95.

15. Tanaka J, Toku K, Zhang B, Ishihara K, Sakanaka M, Maeda N. Astrocytes prevent neuronal death induced by reactive oxygen and nitrogen species. Glia. 1999;28(2):85-96.

16. Kraft AD, Johnson DA, Johnson JA. Nuclear factor E2-related factor 2-dependent antioxidant response element activation by tert-butylhydroquinone and sulforaphane occurring preferentially in astrocytes conditions neurons against oxidative insult. The Journal of neuroscience : the official journal of the Society for Neuroscience. 2004;24(5):1101-12.

17. Loboda A, Damulewicz M, Pyza E, Jozkowicz A, Dulak J. Role of Nrf2/HO-1 system in development, oxidative stress response and diseases: an evolutionarily conserved mechanism. Cellular and molecular life sciences : CMLS. 2016;73(17):3221-47.

18. Buendia I, Michalska P, Navarro E, Gameiro I, Egea J, León R. Nrf2-ARE pathway: An emerging target against oxidative stress and neuroinflammation in neurodegenerative diseases. Pharmacology & therapeutics. 2016;157:84-104.

19. Turpaev KT. Keap1-Nrf2 signaling pathway: mechanisms of regulation and role in protection of cells against toxicity caused by xenobiotics and electrophiles. Biochemistry Biokhimiia. 2013;78(2):111-26.

20. Cullinan SB, Gordan JD, Jin J, Harper JW, Diehl JA. The Keap1-BTB protein is an adaptor that bridges Nrf2 to a Cul3-based E3 ligase: oxidative stress sensing by a Cul3-Keap1 ligase. Molecular and cellular biology. 2004;24(19):8477-86.

21. Bellezza I, Giambanco I, Minelli A, Donato R. Nrf2-Keap1 signaling in oxidative and reductive stress. Biochimica et biophysica acta Molecular cell research. 2018;1865(5):721-33.

22. Al-Sawaf O, Clarner T, Fragoulis A, Kan YW, Pufe T, Streetz K, et al. Nrf2 in health and disease: current and future clinical implications. Clinical science (London, England : 1979). 2015;129(12):989-99.

23. Cordaro M, Casili G, Paterniti I, Cuzzocrea S, Esposito E. Fumaric Acid Esters Attenuate Secondary Degeneration after Spinal Cord Injury. Journal of neurotrauma. 2017;34(21):3027-40.

24. Linker RA, Lee DH, Ryan S, van Dam AM, Conrad R, Bista P, et al. Fumaric acid esters exert neuroprotective effects in neuroinflammation via activation of the Nrf2 antioxidant pathway. Brain : a journal of neurology. 2011;134(Pt 3):678-92.

25. Fragoulis A, Laufs J, Müller S, Soppa U, Siegl S, Reiss LK, et al. Sulforaphane has opposing effects on TNF-alpha stimulated and unstimulated synoviocytes. Arthritis Res Ther. 2012;14(5):R220.

26. Dohlen G, Odland HH, Carlsen H, Blomhoff R, Thaulow E, Saugstad OD. Antioxidant activity in the newborn brain: a luciferase mouse model. Neonatology. 2008;93(2):125-31.

27. Draheim T, Liessem A, Scheld M, Wilms F, Weißflog M, Denecke B, et al. Activation of the astrocytic Nrf2/ARE system ameliorates the formation of demyelinating lesions in a multiple sclerosis animal model. Glia. 2016;64(12):2219-30.

28. Park JH, Kim JH, Oh SK, Baek SR, Min J, Kim YW, et al. Analysis of equivalent parameters of two spinal cord injury devices: the New York University impactor versus the Infinite Horizon impactor. Spine J. 2016;16(11):1392-403.

29. Eddleston M, de la Torre JC, Oldstone MB, Loskutoff DJ, Edgington TS, Mackman N. Astrocytes are the primary source of tissue factor in the murine central nervous system. A role for astrocytes in cerebral hemostasis. J Clin Invest. 1993;92(1):349-58.

30. Alizadeh A, Dyck SM, Karimi-Abdolrezaee S. Traumatic Spinal Cord Injury: An Overview of Pathophysiology, Models and Acute Injury Mechanisms. Front Neurol. 2019;10:282.

31. Bhattacharyya A, Chattopadhyay R, Mitra S, Crowe SE. Oxidative stress: an essential factor in the pathogenesis of gastrointestinal mucosal diseases. Physiol Rev. 2014;94(2):329-54.

32. Tu W, Wang H, Li S, Liu Q, Sha H. The Anti-Inflammatory and Anti-Oxidant Mechanisms of the Keap1/Nrf2/ARE Signaling Pathway in Chronic Diseases. Aging Dis. 2019;10(3):637-51.

33. Fu J, Xu W, Zhang Y, Sun H, Zhao J. Luteolin Modulates the NF-E2-Related Factor 2/Glutamate-Cysteine Ligase Pathway in Rats with Spinal Cord Injury. J Med Food. 2021;24(3):218-25.

34. Chen F, Hu M, Shen Y, Zhu W, Cao A, Ni B, et al. Isorhamnetin promotes functional recovery in rats with spinal cord injury by abating oxidative stress and modulating M2 macrophages/microglia polarization. Eur J Pharmacol. 2021;895:173878.

35. Li D, Tian H, Li X, Mao L, Zhao X, Lin J, et al. Zinc promotes functional recovery after spinal cord injury by activating Nrf2/HO-1 defense pathway and inhibiting inflammation of NLRP3 in nerve cells. Life Sci. 2020;245:117351.

36. Du F, Wang X, Shang B, Fang J, Xi Y, Li A, et al. Gastrodin ameliorates spinal cord injury via antioxidant and anti-inflammatory effects. Acta Biochim Pol. 2016;63(3):589-93.

37. Chen Y, Qin C, Huang J, Tang X, Liu C, Huang K, et al. The role of astrocytes in oxidative stress of central nervous system: A mixed blessing. Cell Prolif. 2020;53(3):e12781.

38. Sofroniew MV. Astrocyte barriers to neurotoxic inflammation. Nat Rev Neurosci. 2015;16(5):249-63.

39. Itoh K, Chiba T, Takahashi S, Ishii T, Igarashi K, Katoh Y, et al. An Nrf2/small Maf heterodimer mediates the induction of phase II detoxifying enzyme genes through antioxidant response elements. Biochem Biophys Res Commun. 1997;236(2):313-22.

40. Lee JM, Johnson JA. An important role of Nrf2-ARE pathway in the cellular defense mechanism. J Biochem Mol Biol. 2004;37(2):139-43.

41. Ishihara Y, Takemoto T, Itoh K, Ishida A, Yamazaki T. Dual role of superoxide dismutase 2 induced in activated microglia: oxidative stress tolerance and convergence of inflammatory responses. J Biol Chem. 2015;290(37):22805-17.

Figures

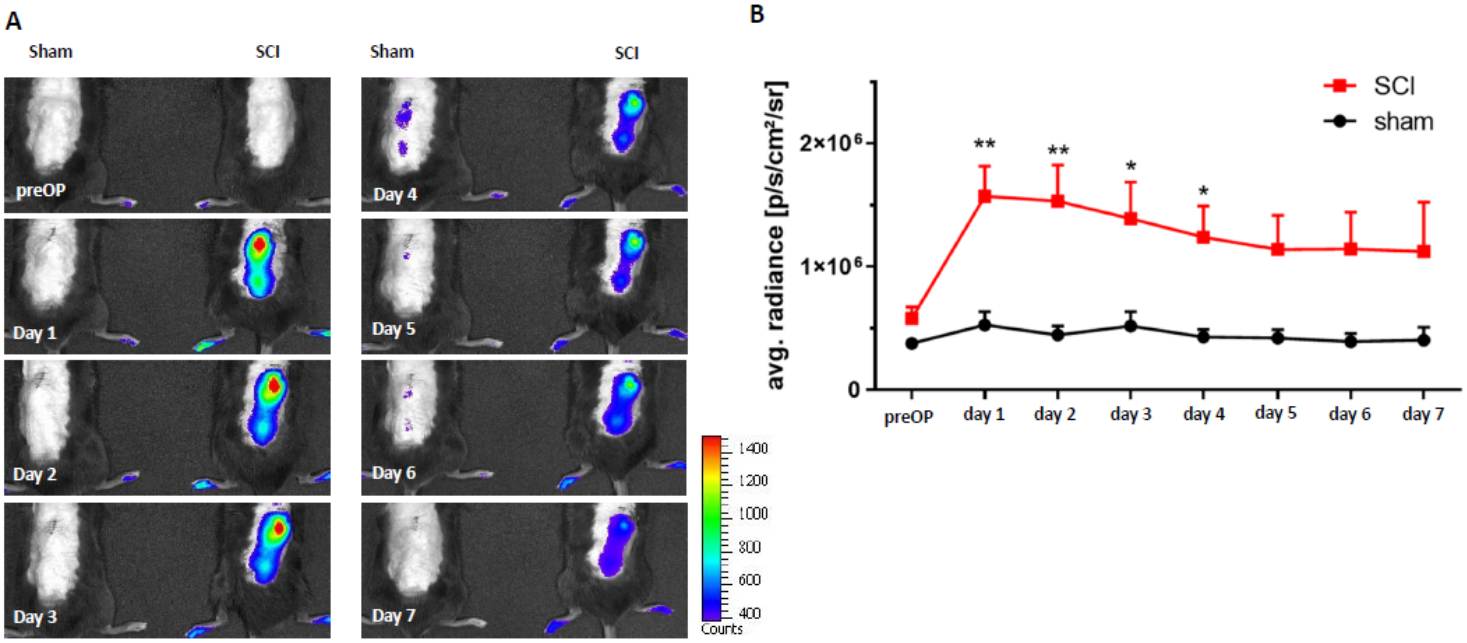

Figure 1

Longitudinal activation pattern of the Nrf2/ARE system in the SCI model. (A) Shows representative pictures of the luminescence measurements of each time point. (B) Quantification of luminescence intensity, depicted as average radiance [photons/second/cm²/steradiant], during the first 7 d post SCI. *p<0.05; **p<0.01 vs. same time point of sham. Data represent means + SD.

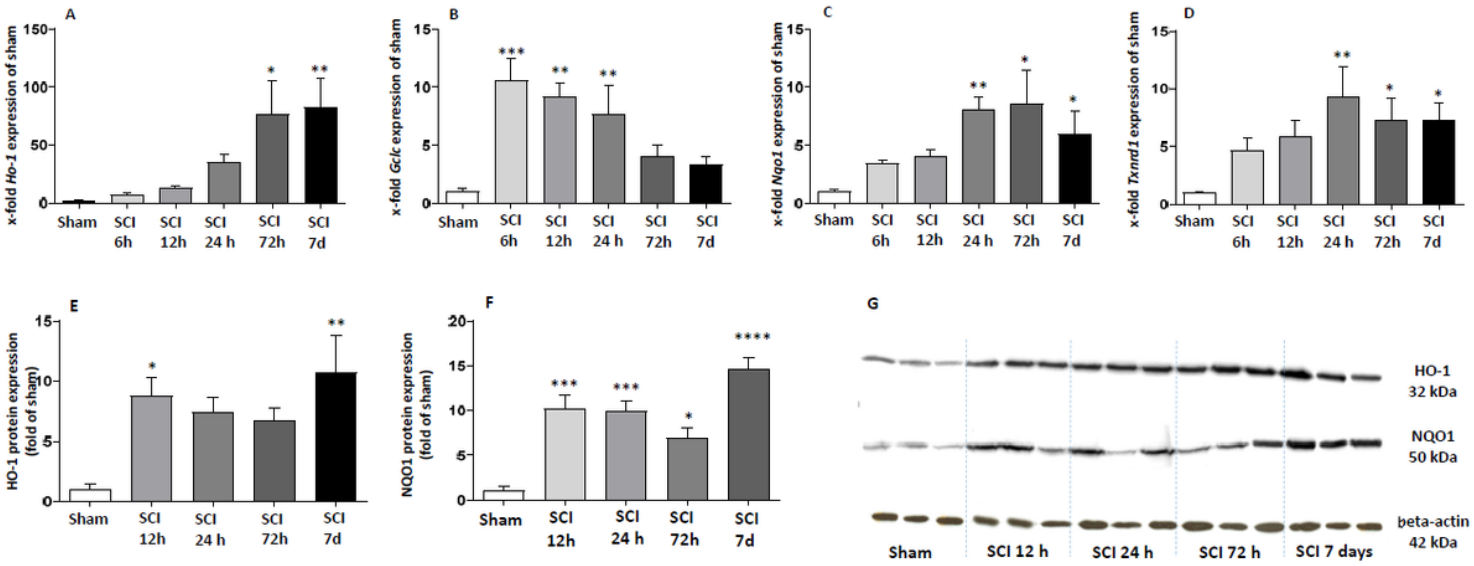

Figure 2

Measurement of Nrf2 target genes. (A-D) Gene expression was investigated using RT-qPCR: HO-1 (heme oxygenase-1), GCLC (glutamate-cysteine ligase, catalytic subunit), NQO1 (NADPH quinone oxidoreductase 1) and TxnRD1 (thioredoxin reductase 1). (E-G) Show the protein levels of HO-1 and NQO1 at 12, 24, 72 h and 7 d post SCI. *p<0.05; **p<0.01,***p<0.001 vs. sham. Data represent means + SEM.

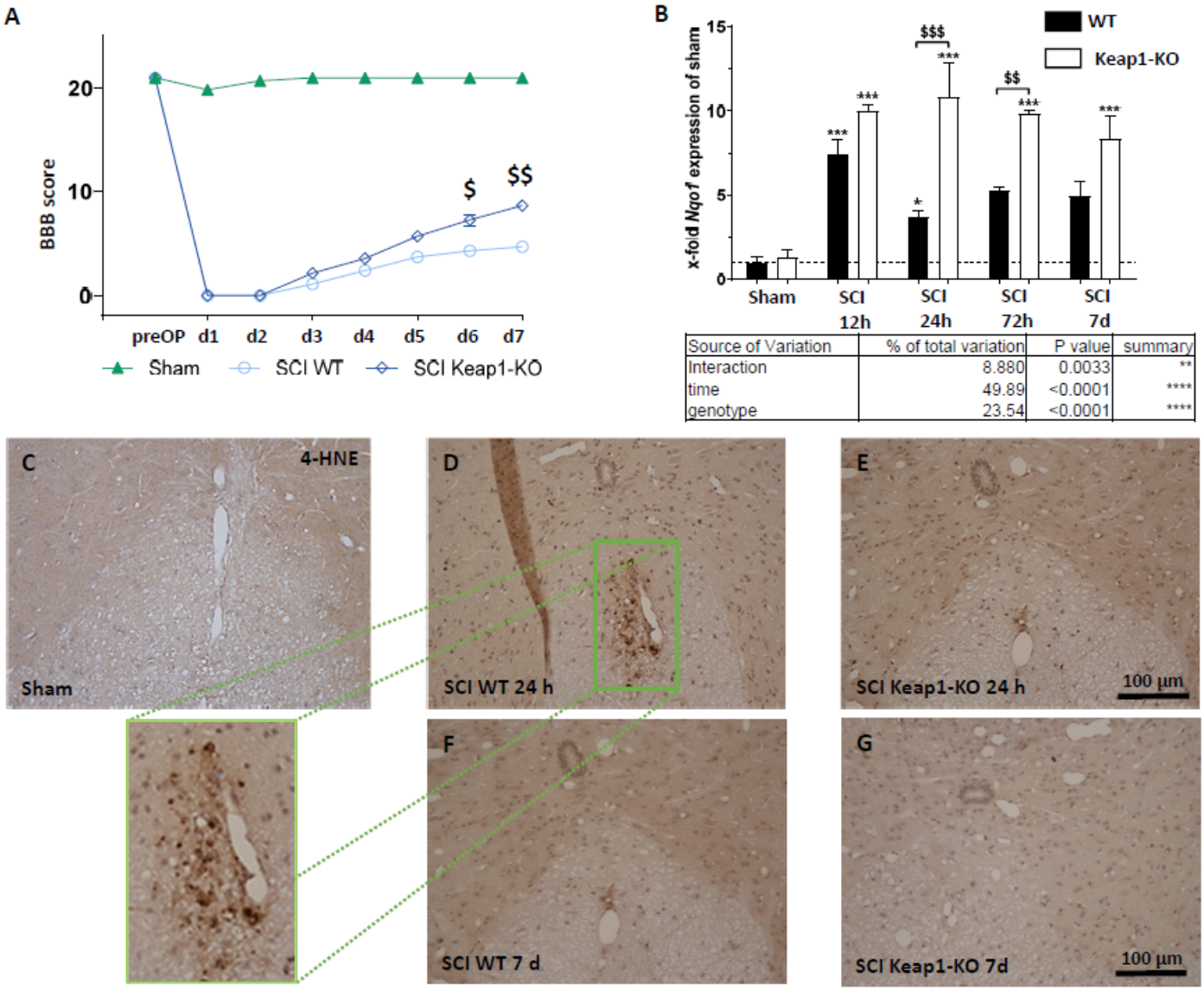

Source of Variation	% of total variation	P value	summary
Interaction	8.880	0.0033	**
time	49.89	<0.0001	****
genotype	23.54	<0.0001	****

Figure 3

Locomotive outcome and oxidative stress after SCI. (A) BBB locomotion test was used to assess the motor function in hind-limbs during the first 7 d after SCI. There was no significant difference from day 1 to 5 between WT and knockout mice. On days 6 and 7, we observed a significantly improved functional recovery in Keap1-KO mice. (B) Shows the gene expression of the Nrf2 target gene Nqo1, in both mice strains and at all investigated time points. sham vs. SCI WT/ SCI Keap1-KO *p<0.05. sham vs. SCI WT/ SCI Keap1-KO ***p<0.001. SCI WT vs. SCI Keap1-KO $p<0.05; SCI WT vs. SCI Keap1-KO

$$p < 0.01. SCIWTvs. SCIKeap1 - KO$$

$p<0.001. Data represent means + SEM. (C-H) Immunhistochemical detection of oxidative stress related damage by the means of 4-Hydroxy-nonenal (4-HNE) after 24h (C-E) and 7 days (F & G) post SCI.

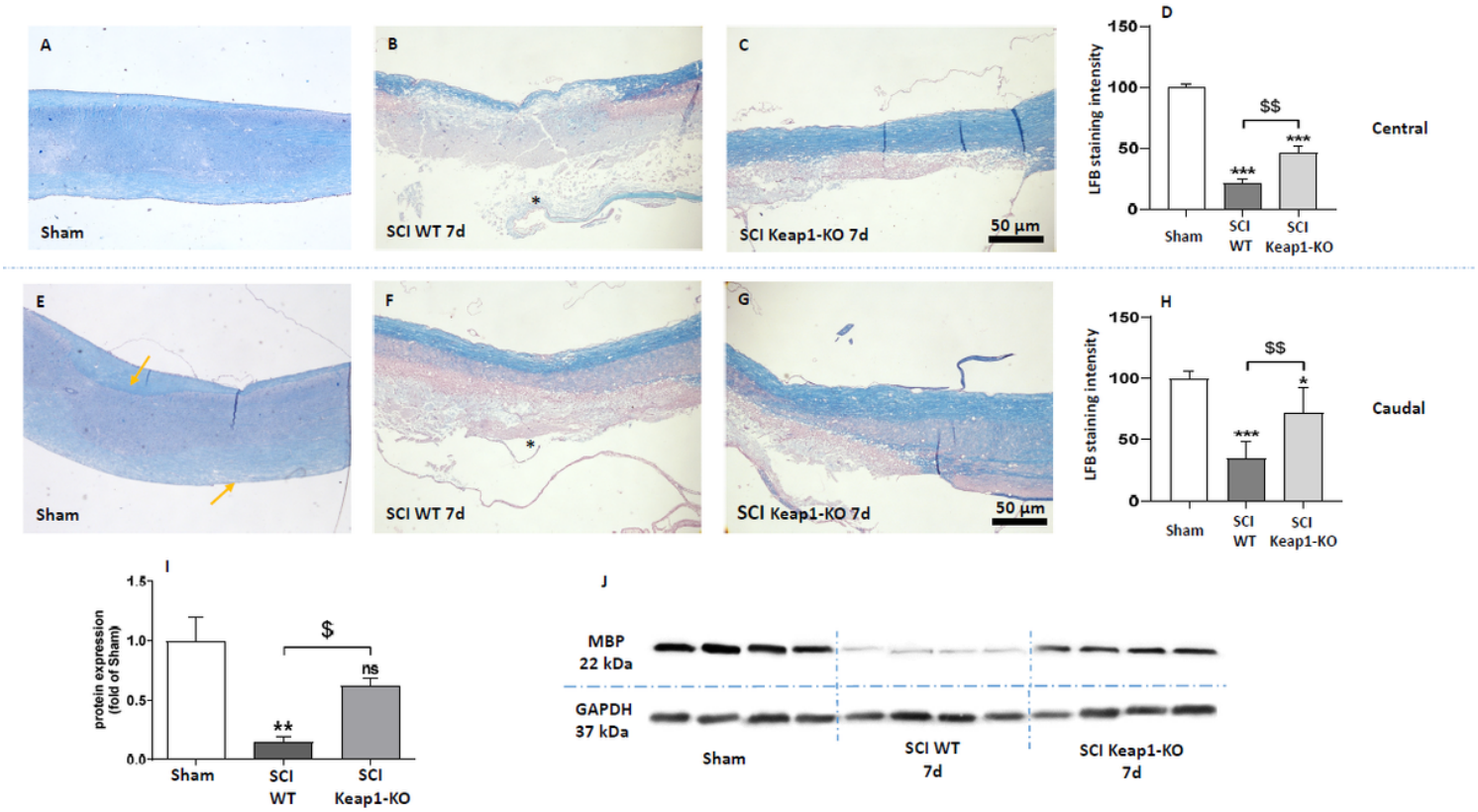

Figure 4

Analyses on myelination and involved proteins. (A-H) Myelin staining intensity (LFB) was markedly reduced in SC post SCI. Nrf2 hyperactivation protected SC from demyelination post SCI in both epicentral (A-D) and caudal (E-H) parts. (I and J) Using western blotting, the amount of myelin basic protein (MBP) (main protein for myelin assembly) was measured in WT and Keap1-KO mice. The myelination index of LFB-stained sections was significantly restored in knockout mice compared to WT animals. Scale bars: 50 µm. sham vs. SCI WT/SCI Keap1-KO *p<0.05. sham vs. SCI WT/SCI Keap1-KO **p<0.01; sham vs. SCI WT/SCI Keap1-KO ***p<0.001; SCI WT vs. SCI Keap1-KO $p<0.05. SCI WT vs. SCI Keap1-KO $$p<0.01. Data represent means ± SEM.

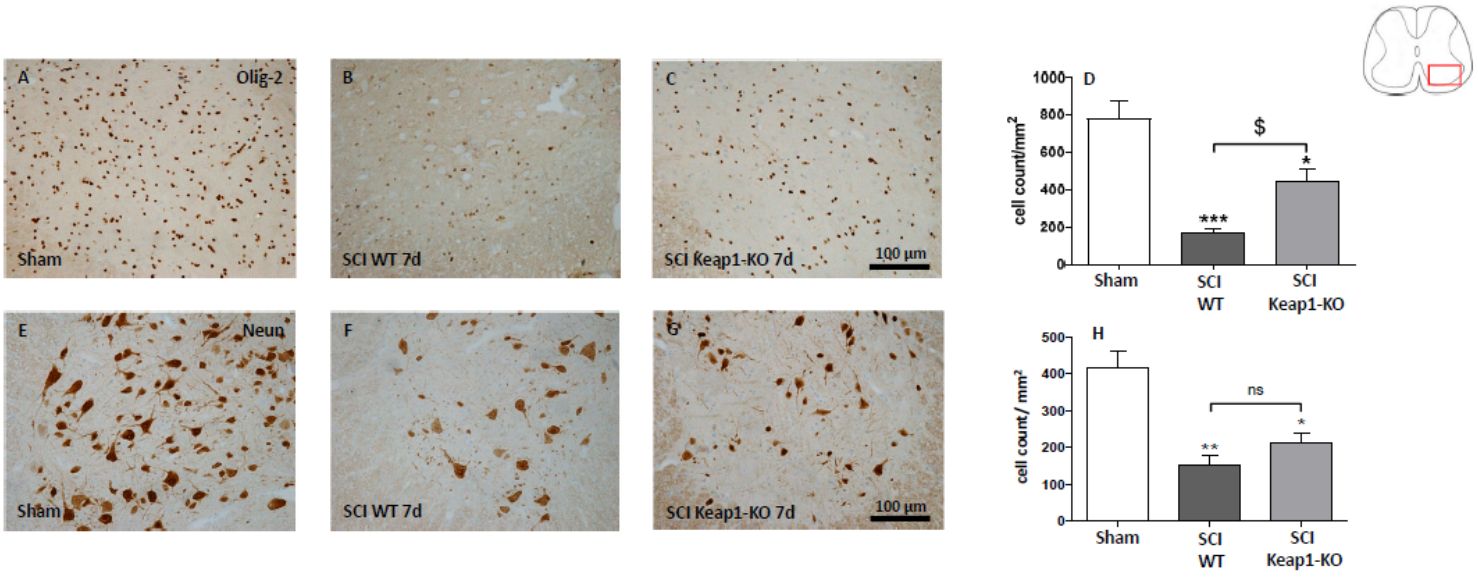

Figure 5

Effect of hyperactivated Nrf2 in astrocytes on oligodendrocytes and neuronal cell numbers post SCI. (A-C) Representative microphotographs of Olig2-positive cells (pan-oligodendrocyte marker) of different experimental groups. (D) Quantification of Olig2-positive cells/mm². The amount of oligodendrocytes is reduced in both genotypes after SCI, but with significantly higher number of remaining Olig2-positive cells in Keap1-KO mice. (E-G) Representative microphotographs of NeuN positive cells (neuronal marker) of different experimental groups. (H) Quantification of NeuN-positive neurons in the ventral horn of the spinal cord is presented in different groups. Scale bars: 100 µm. SCI WT/SCI Keap1-KO *p<0.05. sham vs. SCI WT/SCI Keap1-KO **p<0.01; sham vs. SCI WT/SCI Keap1-KO ***p<0.001.; SCI WT vs. SCI Keap1-KO $p<0.05. Data represent means ± SEM.

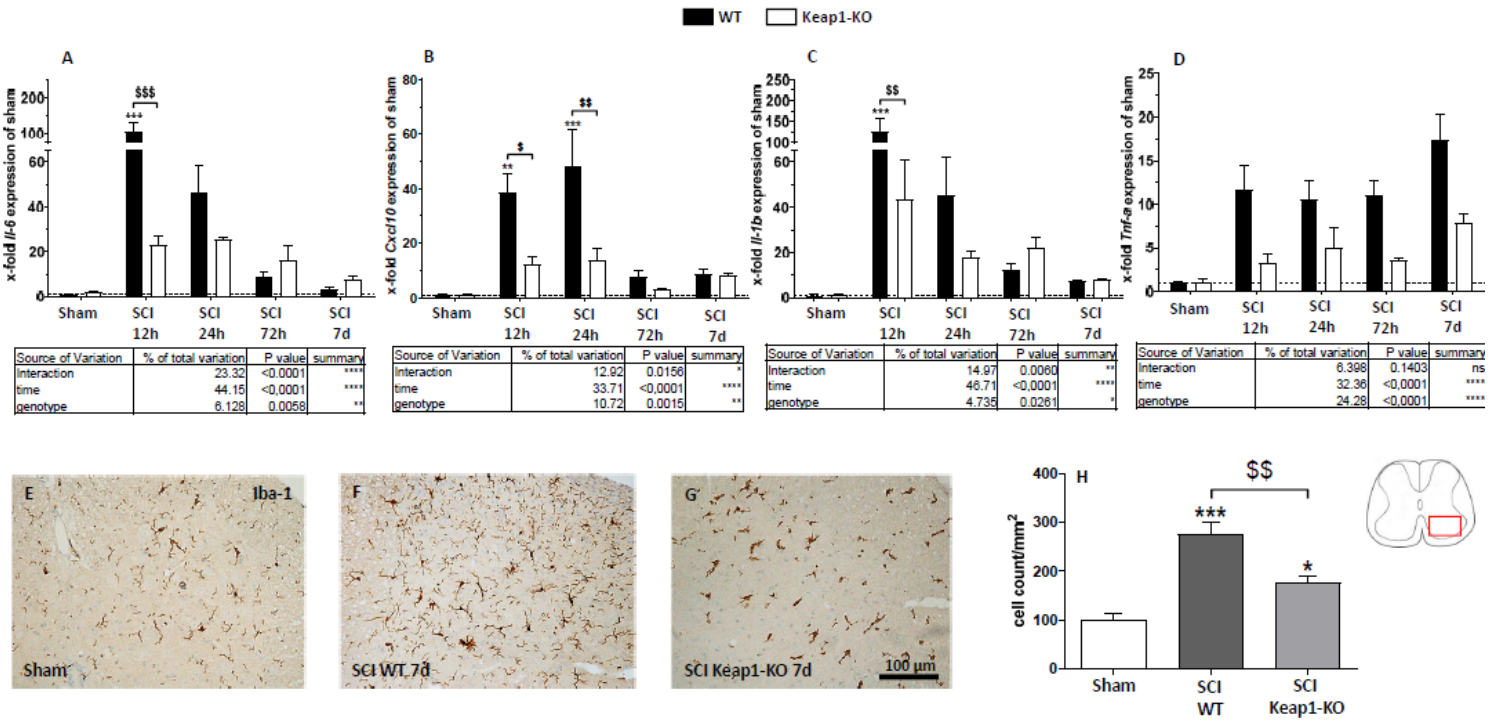

Figure 6

Analyses on neuroinflammatory processes in the course of SCI. (A-D) Regulation of gene expression of different pro-inflammatory cytokines in both WT and Keap1-KO mice at different time points. All measured cytokines, (interleukin 6 (IL-6), C-X-C motif chemokine ligand-10 (CXCL10), interleukin-1b (IL-1b) and tumor necrosis factor alpha (TNF-α)), significantly increased in the early phase post SCI. This effect is partially suppressed in Keap1-KO mice. (E-G) Show the quantitative evaluation of microglia/macrophages (Iba-1) cell numbers in SC 7 days after SCI and representative microphotographs of the different experimental groups. Note that microglia/macrophage responses are significantly reduced in Keap1-KO mice. Scale bars: 100 µm. Sham vs. SCI WT/ SCI Keap1-KO *p<0.05. sham vs. SCI WT/SCI Keap1-KO **p<0.01; sham vs. SCI WT/ SCI Keap1-KO ***p<0.001; SCI WT vs. SCI Keap1-KO $p<0.05; SCI WT vs. SCI Keap1-KO $$p<0.01. Data represent means ± SEM.

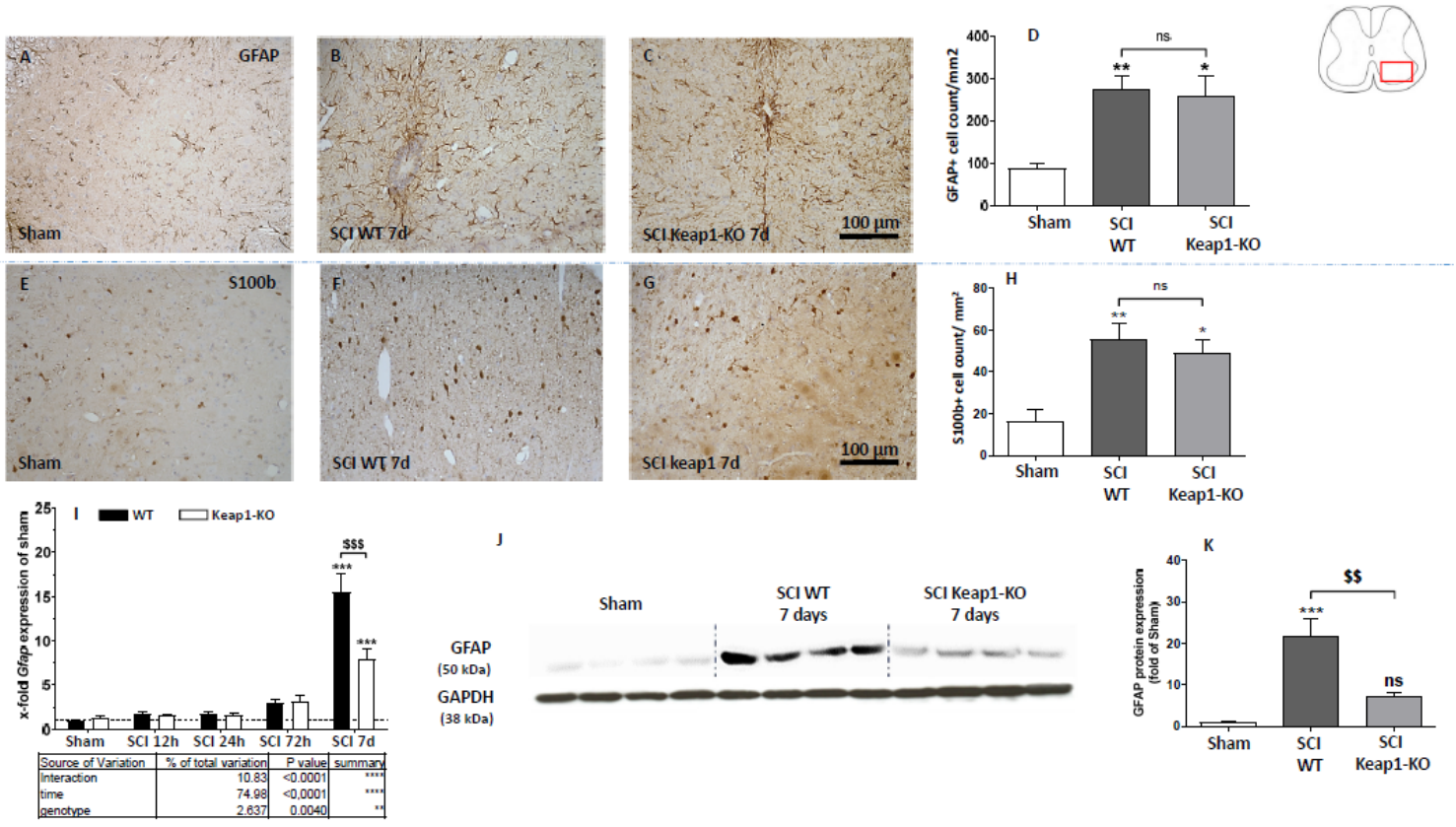

Figure 7

Analyses on astrogliosis and astrocyte reactivity. (A-H) Assessment of number of astrocytes 7 days post SCI using two different markers, GFAP and S100b. SCI induce a significant increase of GFAP- and S100b-positive cells 7 d after SCI. (I) Gene regulation of GFAP in WT and Keap1-KO at different time points. (J-K) Show the protein levels of GFAP in both WT and Keap1-KO mice 7 d post SCI. Scale bars: 100 µm. Sham vs. SCI WT/ SCI Keap1-KO *p<0.05. sham vs. SCI WT/SCI Keap1-KO **p<0.01; sham vs. SCI WT/ SCI Keap1-KO ***p<0.001; SCI WT vs. SCI Keap1-KO

$$p < 0.01. SCIWTvs. SCIKeap1 - KO$$

$p<0.001. Data represent means ± SEM.

Supplementary Files

This is a list of supplementary files associated with this preprint. Click to download.

- Fig.S1detailsonexperimentalsetup.pdf